A new approach to geobarometry by combining fluid inclusion and clumped isotope thermometry in hydrothermal carbonates

Robin Honlet[1], Marta Gasparrini[2], Philippe Muchez[1], Rudy Swennen[1] and Cédric M. John[3]

[1]*Department of Earth and Environmental Sciences, KU Leuven, Celestijnenlaan 200E, 3001 Heverlee, Belgium*

[2]*IFP Energies nouvelles, Georesources Department, Avenue de Bois-Préau 1 & 4, 92852 Rueil-Malmaison Cedex, France*

[3]*Department of Earth Science and Engineering and Qatar Carbonate and Carbon Storage Research Centre, Imperial College London, Prince Consort Road SW7 2BP London, UK*

Corresponding author:

Robin Honlet

Tel.: +32 479 59 19 90

Fax: +32 16 32 29 80

E-mail: robin.honlet@kuleuven.be

Running title :

Geobarometry from diagenetic carbonates

ABSTRACT

This study presents a new approach to geobarometry by combining fluid inclusion and clumped isotope (Δ_{47}) thermometry on carbonate minerals. The offset between homogenization temperatures of primary fluid inclusions with known composition and Δ_{47} temperatures of the host mineral allows a direct estimation of the fluid pressure at the time of carbonate crystallization. This new approach is illustrated via hydrothermal dolomite samples from the Variscan foreland fold-and-thrust belt in northern Spain. Clumped isotope analyses yield crystallization temperatures (107-168 °C) which are higher compared to homogenization temperatures in corresponding samples (95-145 °C). The calculated pressure values suggest that dolomitizing fluids were overpressured during formation of zebra dolomite textures, whereas lower pressures are obtained for dolomite cement from breccia textures. This new approach to geobarometry opens up the possibility of estimating the pressure of carbonate crystallization and has potential applications in diagenesis, basin analysis, ore geology and tectonics.

INTRODUCTION

Pressure is an important parameter to be considered when investigating a wide range of geological processes. Geobarometry can yield information on diagenesis, basin evolution, hydrocarbon generation and boiling of ore-forming fluids, among others. To date, only a limited number of geobarometers exist, only a few of which are applicable to sedimentary and diagenetic settings. Most of these geobarometers are, at least partly, based on the use of fluid inclusion (FI) data (Roedder and Bodnar, 1980). One way to estimate pressure conditions during crystal growth is by combining information from two immiscible fluids which are trapped simultaneously (e.g. petroleum and aqueous fluids; Munz, 2001). This approach is hampered by the need for multiple

cogenetic FI generations, which are not frequently encountered. If only one generation of inclusions is present, information on its homogenization temperature and composition can be used for geobarometry, but only in combination with an independent geothermometer which can provide the temperature of formation of the host crystal (e.g. chlorite thermometry; Schroyen and Muchez, 2000). An important assumption is that both FIs and mineral phases used as independent geothermometers are spatially and temporally associated, which is not easy to prove (Roedder and Bodnar, 1980).

This study presents a new approach to geobarometry by combining aqueous FI microthermometry with the technique of carbonate clumped isotope (CI) paleothermometry (Δ_{47}; Ghosh *et al.*, 2006). Homogenization temperatures (T_h) obtained from hydrothermal dolomite samples are compared to crystallization temperatures ($T\Delta_{47}$) obtained by measuring the abundance of ^{13}C-^{18}O bonds in the mineral lattice. On the assumption that both FI and CI signatures are pristine and have not been reset, the offset (ΔT) between both temperature sets can be explained by the fact that T_h represents the minimum temperature of FI entrapment while $T\Delta_{47}$ represents the true temperature of crystallization of the host dolomite mineral (figure 1). ΔT is influenced by the pressure at the time of inclusion entrapment, referred to as the pressure correction (Goldstein, 2001). Hence, it can give a direct estimate of pressure at the time of dolomite crystallization, without the need for cogenetic FI generations or other types of geothermometers, since both temperatures are obtained from the same carbonate mineral phase.

GEOLOGICAL SETTING

The Cantabrian Zone (CZ) represents the Variscan foreland fold-and-thrust belt (FFTB) on the Iberian Peninsula (Julivert, 1971). Carbonate production prevailed in the foreland basin during

71 the Mississippian and Early Pennsylvanian, following an important marine transgression. One of
72 the most common Carboniferous limestone formations in the CZ is the Serpukhovian Barcaliente
73 Formation (Fm.), composed of thinly bedded dark carbonate mudstones (Wagner *et al.*, 1971).
74 The Paleozoic successions of the CZ were folded and thrusted into an east-verging FFTB during
75 Moscovian times (Alonso *et al.*, 2009). The original N-S oriented mountain range evolved into a
76 thick-skinned secondary orocline during the Late Carboniferous (ca. 310-297 Ma; Gutiérrez-
77 Alonso *et al.*, 2015). Following oroclinal buckling, the thickened lithosphere underneath the
78 center of the orocline (corresponding to the CZ) became unstable, detached and sunk away
79 resulting in upwelling of hot asthenospheric material (ca. 295-285 Ma; Valverde-Vaquero *et al.*,
80 1999). The upwelling created near-surface uplift and extension as well as an increase in crustal
81 heat flow (Weil *et al.*, 2013).
82 As a result, hypersaline marine-derived brines infiltrated the subsurface along reactivated
83 Variscan fractures in the Bodón Unit, an important thrust unit in the CZ (figure 2; Julivert, 1971;
84 Gasparrini *et al.*, 2006a). These brines were modified through water-rock interactions and the
85 resulting hydrothermal fluids dolomitized Paleozoic limestones through thermal convection
86 (Gasparrini *et al.*, 2006a; Honlet *et al.*, in press). Inclusions within the dolomite crystals are two-
87 phase aqueous with consistent liquid to vapor ratios. FI microthermometry on void-filling
88 dolomite yielded T_h values between 110 to 150°C (Gasparrini *et al.*, 2006b). Salinity calculations
89 based on microthermometry coupled with cryo-Raman spectroscopy revealed salinities around
90 26 eq. wt% $CaCl_2$ (Gasparrini *et al.*, 2006b). Raman spectroscopic measurements on the gas
91 bubbles did not detect gases such as CO_2, CH_4 or N_2 (Gasparrini, 2003). Hydrothermal fluid
92 circulation was the hottest event affecting the Paleozoic rocks of the CZ, based on apatite fission-
93 track (AFT) thermochronology (Carrière, 2006).

METHODS

Our dataset consists of 7 new samples and 2 samples provided by Gasparrini *et al.* (2006b; table 1). All samples were collected from the Barcaliente Fm. exposed in the Bodón Unit, from locations (figure 2) that correspond to those of Gasparrini *et al.* (2006b).

Samples and thin sections were investigated with plane light microscopy (Leica DM LP microscope) and cathodoluminescence microscopy (Techosyn Model 8200 Mark II instrument mounted on a Nikon microscope).

In order to obtain a precise comparison between T_h and $T\Delta_{47}$, new FI measurements were performed on all samples, including those provided by Gasparrini *et al.* (2006b). Inclusions suitable for microthermometric analysis were selected based on a petrographic study of both thin sections and double polished thick sections (± 100 µm thick; cold-polishing technique; cf. Muchez *et al.*, 1994). Measurements were carried out on a Linkam MDS-600 heating/cooling stage mounted on an Olympus BX51 microscope. The stage was calibrated by synthetic Syn Flinc^{Tm} FI standards. Isochores were calculated for each sample using salinity data from Gasparrini *et al.* (2006b) and the equation of state of Zhang and Frantz (1987).

Clumped isotope analyses were performed in the Qatar Stable Isotope Lab at Imperial College London. The method used for the analyses is based on Dennis and Schrag (2010) and described for the Imperial College laboratory in Dale *et al.* (2014). Powder samples were drilled from rock slabs using a dental drilling device. On average 3 to 5 replicate measurements were performed for each sample using the same manual CO_2 purification line and mass spectrometer. Aliquots of 5 to 6 mg of dolomite powder were digested online in a phosphoric acid bath held at 90°C for 20 minutes to allow complete reaction. The liberated CO_2 gas was subsequently purified and measured on a Thermo Fisher MAT 253 isotope ratio mass spectrometer. Data processing was

performed using the free software Easotope (John and Bowen, 2016). Non-linearity corrections were done based on heated gases (Huntington *et al.*, 2009), and the projection of the data into the absolute reference frame of Dennis *et al.* (2011) was performed using heated gases and inter-laboratory standards Carrara marble, ETH2 and ETH3 (Meckler *et al.*, 2014; average SE between 0.0025 and 0.0054‰). All data are presented in the absolute reference scale (CDES) using the permil (‰) unit. Reliability of the measurements was assessed based on the Δ_{48} offset and 49 parameter (cf. Huntington *et al.*, 2009). Δ_{47} values were converted into temperatures using the Kluge *et al.* (2015) calibration, reprocessed using the "Brand" parameters for ^{17}O correction (Daëron *et al.*, 2016). The Kluge *et al.* (2015) calibration, which is based on calcite, has been shown to be indistinguishable from several other calibrations (Petersen *et al.*, 2017), including calibrations based on dolomite (Bonifacie *et al.*, 2017). Temperatures are reported at 1 standard error (SE) precision and at 95% confidence level (CL).

RESULTS

Dolomite samples display zebra or breccia textures. Zebra textures (figure 3A) have been formerly interpreted as alternations of dark gray replacive and white dolomite cement filling voids developed by focused flow of overpressured basinal fluids (Nielsen *et al.*, 1998; Vandeginste *et al.*, 2005). The dolomite veins making up zebra sets in the samples used for this study consist of thin rims made up of idiotopic white dolomite crystals (figure 3B). They show a mottled appearance under the cathodoluminescence microscope, except for a last growth zone exhibiting a dull luminescence (figure 3C). Breccia occurs as pockets (figure 3D) composed of angular fragments of replacive dolomite in a matrix of dolomite and calcite cement (figure 3E). They are mostly clast-supported, with thick dolomite cement rims which show a luminescence

similar to the rims observed in zebra veins (figure 3F). Individual dolomite crystals are larger compared to those making up the zebra veins, though they show stepwise crystal terminations. The dull rims in both zebra and breccia textures show signs of dedolomitization, and were avoided during sampling prior to measurements. Two breccia samples (samples 202 and CaBD2B) are coarse crystalline and show an orange weathering patina (figure 3G), which suggests a strong enrichment in Fe. They are made up of replacive dolomite with large crystal sizes (around 250 µm; figure 3H) and abundant development of saddle dolomite crystals (up to 2000 µm; figure 3I). Both replacive and void-filling dolomite in these samples are non-luminescent.

FIs were carefully selected to avoid analysis of secondary inclusions. Primary inclusions, with sizes generally between 4 and 10 µm, were selected from petrographically associated assemblages (FIA; Goldstein and Reynolds, 1994) and from growth zones within individual crystals. T_h modes broadly correspond to those obtained by Gasparrini *et al.* (2006b) and range between 95 and 145°C (figure 4; table 1). Frequency histograms of T_h data for individual samples show unimodal distributions.

Clumped isotope Δ_{47} temperatures obtained from dolomite crystals range between 107 and 168 °C (figure 4; table 1). For 8 out of 9 samples investigated, the $T\Delta_{47}$ are higher compared to T_h-values. External precisions range between ±1 and ±8°C (±1SE). The error margins at 95% CL are on average 3 to 4 times higher compared to SE, but could be reduced with additional measurements.

DISCUSSION

Fluid inclusions *versus* clumped isotopes

Several sources of error can influence both FI and CI datasets and can result in significant variations. Fluid inclusions should be primary and not affected by post-entrapment processes such as thermal reequilibration or crystal deformation (Goldstein and Reynolds, 1994). The carbonate crystals should not be affected by solid-state diffusion of O and C atoms, which could induce an overestimation of the clumped isotope signature (Came *et al.*, 2017). Solid-state diffusion is a molecular-scale diffusion process whereby atoms can migrate through a crystal when it is exposed to high temperatures (Dennis and Schrag, 2010; Passey and Henkes, 2012). Temperatures necessary for diffusion likely approach 300°C for dolomite (MacDonald *et al.*, 2017; Lloyd *et al.*, 2017). Hydrothermal dolomitization was the hottest event affecting the Paleozoic rocks in the CZ (Carrière, 2006) excluding the possibility of solid-state diffusion.

A secondary cause which could account for part of the temperature variation between clumped isotopes and FIs is the difference in the sample volumes for both techniques. Powder samples used for clumped isotope analyses were drilled from dolomite crystals visible on rock slabs and are inevitably derived from a suite of crystals (Defliese and Lohmann, 2015). FI measurements, on the other hand, allow obtaining T_h-values for individual crystals and growth zones. Hydrothermal systems are known to be episodically very dynamic (Eichhubl and Boles, 2000), which may account for rapid variations in temperature. FI data obtained from individual crystals might therefore differ from clumped isotope data which give an "averaged" temperature. Analytical improvements resulting in increasingly small sample sizes will allow more precise clumped isotope measurements (Hu *et al.*, 2014; Müller *et al.*, 2017).

Geobarometry

The CI dataset yields crystallization temperatures between 107 and 168 °C, which can be plotted on the isochores constructed for each sample based on their T_h mode and composition of their

FIs (figure 5). Corresponding pressures range between 0 and 72 MPa. Void-filling dolomite cement from breccia samples is characterized by low pressures (0-8 MPa), while dolomite crystals in zebra veins formed at higher pressures, between 29 to 72 MPa. The lower pressures recorded by breccia cements could be related to an abrupt decrease in fluid pressure that results from the creation of open space following hydraulic brecciation (Knipe, 1993). The massive nature of the cements and their imperfect crystal morphologies (e.g. stepwise crystal terminations) support a model of fast precipitation in response to a sudden decrease in fluid pressure. The higher overpressures recorded for dolomite crystals forming zebra veins support the idea that zebra textures form during a pre-seismic buildup of suprahydrostatic to supralithostatic pressures (Nielsen *et al.*, 1998; Muchez and Sintubin, 2002). These overpressures are also in agreement with the relatively new view on zebra textures introduced by Merino *et al.* (2006), stating that zebra textures are self-organized, pushing aside replacive dolomite through pressure-dissolution. Dolomite rhombs displace the host constituents due to local induced stress generated by crystal growth. This induced stress can reach 47 MPa for dolomite crystals growing at 100°C (Merino *et al.*, 2006). The breccia samples (CaBD2B and 202) composed of coarse saddle crystals lacking luminescence are characterized by higher pressures compared to pristine breccia (figure 5). These two samples might originate from a separate episode of faulting and expulsion of dolomitizing fluids resulting in coarse crystalline dolomitization or recrystallization of the initial dolomite rocks. The observed temperatures and pressures are thus not representative of the initial crystallization process, but of a later pulse of dolomitization or recrystallization.

The dataset used in this study illustrates the potential power of coupled T_h-$T\Delta_{47}$ geobarometry in carbonate minerals, suggesting a high pressure for zebra dolomite formation in the study area.

Additional measurements on dolomite exposures in different geodynamic settings would allow generalization towards regional processes.

CONCLUSIONS

Hydrothermal dolomite samples from the Cantabrian Zone (northern Spain) have been used to test a new geobarometry approach by combining fluid inclusion and clumped isotope thermometry. This approach allows an estimation of the pressure during crystallization of carbonate minerals, without the need for cogenetic generations of FIs or the use of independent geothermometers. Clumped isotope temperatures (107-168 °C) of dolomite crystals from zebra and breccia textures are higher compared to fluid inclusion homogenization temperatures from the same samples (95-145 °C). The offset between these values mainly depends on the pressure during FI entrapment. Zebra dolomite likely formed during pre-seismic pressure buildup (29-72 MPa), while dolomite cement in breccia samples precipitated in response to a sudden decrease in fluid pressures upon fault rupture. Geobarometry based on fluid inclusion and clumped isotope thermometry is not only a promising tool for carbonate diagenesis studies, but could prove useful for a broad range of geological applications.

ACKNOWLEDGEMENTS

R. Honlet is supported by Research Foundation - Flanders. C. John acknowledges support from the Qatar Carbonate and Carbon Storage Research Center for the clumped isotopes laboratory, funded by Qatar Petroleum, Shell, and the Qatar Science and Technology Park. E. Bemer (IFPEN) is thanked for supporting the involvement of M. Gasparrini.

REFERENCES CITED

Alonso, J.L., Marcos, A. and Suárez, A., 2009. Paleogeographic inversion resulting from large out of sequence breaching thrusts : The León Fault (Cantabrian Zone, NW Iberia). A new picture of the external Variscan Thrust Belt in the Ibero-Armorican Arc. *Geologica Acta*, **7**, 451-473.

Bonifacie, M., Calmels, D., Eiler, J.M., Horita, J., Chaduteau, C., Vasconcelos, C., Agrinier, P., Katz, A., Passey, B.H., Ferry, J.M. and Bourrand, J.J., 2017. Calibration of the dolomite clumped isotope thermometer from 25 to 350°C, and implications for a universal calibration for all (Ca, Mg, Fe)CO_3 carbonates. *Geochimica et Cosmochimica Acta,* **200,** 255-279.

Came, R.E., Azmy, K., Tripati, A. and Olanipekun, B.J., 2017. Comparison of clumped isotope signatures of dolomite cements to fluid inclusion thermometry in the temperature range of 73-176 °C. *Geochimica et Cosmochimica Acta*, **199**, 31-47.

Carrière, K.L., 2006. Neoproterozoic to Holocene tectonothermal evolution of the southern Cantabrian Mountains NW Iberia, revealed by apatite fission-track thermochronology. Unpubl. doctoral dissertation, Ruprecht-Karls-Universität, Heidelberg, 270 pp.

Daëron, M., Blamart, D., Peral, M. and Affek, H.P., 2016. Absolute isotopic abundance ratios and the accuracy of Δ47 measurements. *Chemical Geology*, **442**, 83-96.

Dale, A., John, C.M., Mozley, P.S., Smalley, P.C. and Muggeridge, A.H., 2014. Time-capsule concretions: Unlocking burial diagenetic processes in the Mancos Shale using carbonate clumped isotopes. *Earth and Planetary Science Letters*, **394**, 30-37.

Defliese, W.F. and Lohmann, K.C., 2015. Non-linear mixing effects on mass-47 CO_2 clumped isotope thermometry: Patterns and implications. *Rapid Communications in Mass Spectrometry*, **29**, 901-909.

255 Dennis, K.J. and Schrag, D.P., 2010. Clumped isotope thermometry of carbonatites as an indicator
256 of diagenetic alteration. *Geochimica et Cosmochimica Acta*, **74**, 4110-4122.
257 Dennis, K.J., Affek, H.P., Passey, B.H., Schrag, D.P. and Eiler, J.M., 2011. Defining an absolute
258 reference frame for 'clumped' isotope studies of CO_2. *Geochimica et Cosmochimica Acta*, **75**,
259 7117-7131.
260 Eichhubl, P. and Boles, J.R., 2000. Rates of fluid flow in fault systems – Evidence for episode
261 rapid fluid flow in the Miocene Monterey Formation, coastal California. *American Journal of*
262 *Science*, **300**, 571-600.
263 Gasparrini, M., 2003. Large-scale hydrothermal dolomitisation in the southwestern Cantabrian
264 Zone (NW Spain): causes and controls of the process and origin of the dolomitizing fluids.
265 Unpubl. doctoral dissertation, Ruprecht-Karls-Universität, Heidelberg, 193 pp.
266 Gasparrini, M., Bechstädt, T. and Boni, M., 2006a. Massive hydrothermal dolomites in the
267 southwestern Cantabrian Zone (Spain) and their relation to the Late Variscan evolution.
268 *Marine and Petroleum Geology*, **23**, 543-568.
269 Gasparrini, M., Bakker, R.J. and Bechstädt, T., 2006b. Characterization of dolomitizing fluids in
270 the Carboniferous of the Cantabrian Zone (NW Spain): a fluid-inclusion study with cryo-
271 raman spectroscopy. *Journal of Sedimentary Research*, **76**, 1304-1322.
272 Ghosh, P., Adkins, J., Affek, H., Balta, B., Guo, W., Schauble, E.A., Schrag, D. and Eiler, J.M.,
273 2006. ^{13}C-^{18}O bonds in carbonate minerals: A new kind of paleothermometer. *Geochimica et*
274 *Cosmochimica Acta*, **70**, 1439-1456.
275 Goldstein, R.H., 2001. Fluid inclusions in sedimentary and diagenetic systems. *Lithos*, **55**, 159-
276 193.

277 Goldstein, R.H. and Reynolds, T.J., 1994. Systematics of fluid inclusions in diagenetic minerals.
278 *Society for Sedimentary Geology Short Course*, **31**, 199 pp.
279 Gutiérrez-Alonso, G., Collins, A.S., Fernández-Suárez, J., Pastor-Galán, D., González-Clavijo, E.,
280 Jourdan, F., Weil, A.B. and Johnston, S.T., 2015. Dating of lithospheric buckling: $^{40}Ar/^{39}Ar$
281 ages of syn-orocline strike-slip shear zones in northwestern Iberia. *Tectonophysics*, **643**, 44-
282 54.
283 Honlet, R., Gasparrini, M., Jäger, H., Muchez, Ph. and Swennen, R., in press. Precursor and
284 ambient rock paleothermometry to assess the thermicity of burial dolomitization in the
285 southern Cantabrian Zone (northern Spain). *International Journal of Earth Sciences*, doi:
286 10.1007/s00531-017-1541-2.
287 Hu, B., Radke, J., Schlüter, H.J., Heine, F.T., Zhou, L. and Bernasconi, S.M., 2014. A modified
288 procedure for gas-source isotope ratio mass spectrometry: the long-integration dual-inlet
289 (LIDI) methodology and implications for clumped isotope measurements. *Rapid*
290 *Communications in Mass Spectrometry*, **28**, 1413-1425.
291 Huntington, K.W., Eiler, J.M., Affek, H.P., Guo, W., Bonifacie, M., Yeung, L.Y., Thiagarajan,
292 N., Passey, B., Tripati, A., Daëron, M. and Came, R., 2009. Methods and limitations of
293 'clumped' CO_2 isotope (Δ_{47}) analysis by gas-source isotope ratio mass spectrometry.
294 *Journal of Mass Spectrometry*, **44**, 1318-1329.
295 John, C.M. and Bowen, D., 2016. Community software for challenging isotope analysis: First
296 applications of 'Easotope' to clumped isotopes. *Rapid Communications in Mass*
297 *Spectrometry*, **30**, 2285-2300.
298 Julivert, M., 1971. Décollement tectonics in the Hercynian Cordillera of northwest Spain.
299 *Americal Journal of Science*, **270**, 1-29.

300 Knipe, R.J., 1993. The influence of fault zone processes and diagenesis on fluid flow. In:
301 *Diagenesis and Basin Development* (A.D. Horbury and A.G. Robinson, eds.). *AAPG Studies*
302 *in Geology*, **36**, 135-151.
303 Kluge, T., John, C.M., Jourdan, A.L., Davis, S. and Crawshaw, J., 2015. Laboratory calibration of
304 the calcium carbonate clumped isotope thermometer in the 25-250°C temperature range.
305 *Geochimica et Cosmochimica Acta*, **157**, 213-227.
306 Lloyd, M.K., Eiler, J.M. and Nabelek, P.I., 2017. Clumped isotope thermometry of calcite and
307 dolomite in a contact metamorphic environment. *Geochimica et Cosmochimica Acta*, **197**,
308 323-344.
309 MacDonald, J.M., John, C.M. and Girard, J.P., 2017. Testing clumped isotopes as a reservoir
310 characterization tool: a comparison with fluid inclusions in a dolomitized sedimentary
311 carbonate reservoir buried to 2-4 km. In: *From Source to Seep: Geochemical Applications in*
312 *Hydrocarbon Systems* (M. Lawson, ed). *Geological Society of London* (in press).
313 Meckler, A., Ziegler, M., Millán, M., Breitenbach, S. and Bernasconi, S., 2014. Long-term
314 performance of the Kiel carbonate device with a new correction scheme for clumped isotope
315 measurements. *Rapid Communications in Mass Spectrometry*, **28**, 1705-1715.
316 Merino, E., Canals, A. and Fletcher, R.C., 2006. Genesis of self-organized zebra textures in
317 burial dolomites: Displacive veins, induced stress, and dolomitization. *Geologica Acta*, **4**,
318 383-393.
319 Muchez, Ph., Marshall, J.D., Touret, J.L.R. and Viaene, W.A., 1994. Origin and migration of
320 palaeofluids in the Upper Visean of the Campine Basin, northern Belgium. *Sedimentology*,
321 **41**, 133-145.

Muchez, Ph. and Sintubin, M., 2002. Palaeofluid flow within the evolution of sedimentary basins: principles and examples from the Carboniferous of Belgium. *Aardkundige Mededelingen*, **12**, 161-164.

Müller, I.A., Fernandez, A., Radke, J., van Dijk, J., Bowen, D., Schwieters, J. and Bernasconi, S.M., 2017. Carbonate clumped isotope analyses with the long-integration dual-inlet (LIDI) workflow: scratching at the lower sample weight boundaries. *Rapid Communications in Mass Spectrometry*, **31**, 1057-1066.

Muñoz Quijano, I.N., 2015. Hydrothermal dolomitization of Paleozoic successions in Northern Spain : petrophysical properties and structural control. Unpubl. doctoral dissertation, Ruprecht-Karls-Universität, Heidelberg, 239 pp.

Munz, I.A., 2001. Petroleum inclusions in sedimentary basins: systematics, analytical methods and applications. *Lithos*, **55**, 195-212.

Nielsen, P., Swennen, R., Muchez, Ph. and Keppens, E., 1998. Origin of Dinantian zebra dolomites south of the Brabant-Wales Massif, Belgium. *Sedimentology*, **45**, 727-743.

Passey, B.H. and Henkes, G.A., 2012. Carbonate clumped isotope bond reordering and geospeedometry. *Earth and Planetary Science Letters*, **351-352**, 223-236.

Petersen, S.V., Daëron, M., Defliese, W.F., John, C.M., Bernasconi, S.M., Colman, A.S., Huntington, K.W., Kelson, J.R., Kluge, T., Olack, G.A., Saenger, C., Schauer, A.J., Bajnai, D., Bonifacie, M., Fiebig, J., Fernandez, A.B., Garcia de Real, P., Henkes, G.A., Katz, A., Kele, S., Lohmann, K.C., Passey, B.H., Petrizzo, D.A., Rosenheim, B.E., Tang, J., Tripati, A.E., Venturelli, R., Young, E.D., Wacker, U. and Winkelstern, I.Z., 2017. Continued efforts towards a universal clumped isotope calibration: updating published calibrations to

Brand et al. (2010) parameters. *International Workshop on Clumped Isotopes*, Paris, August 2017.

Roedder, E. and Bodnar, R.J., 1980. Geological pressure determinations from fluid inclusion studies. *Ann. Rev. Earth Planet. Sci.*, **8**, 263-301.

Schroyen, K. and Muchez, Ph., 2000. Evolution of metamorphic fluids at the Variscan fold-and-thrust belt in eastern Belgium. *Sedimentary Geology*, **131**, 163-180.

Valverde-Vaquero, P., Cuesta-Fernández, A., Gallastegui, G., Suárez, O., Corretgé, L.G. and Dunning, G.R., 1999. U-Pb dating of late-Variscan magmatism in the Cantabrian Zone (northern Spain). *EUG X*, Strasbourg, 101 pp.

Vandeginste, V., Swennen, R., Gleeson, S.A., Ellam, R.M., Osadetz, K. and Roure, F., 2005. Zebra dolomitization as a result of focused fluid flow in the Rocky Mountains Fold and Thrust Belt, Canada. *Sedimentology*, **52**, 1067-1095.

Wagner, R.H., Winkler Prins, C.F. and Riding, R.E., 1971. Lithostratigraphic units of the lower part of the Carboniferous in Northern León, Spain. *Universidad de Oviedo Trabajos de Geología*, **4**, 603-663.

Weil, A.B., Gutiérrez-Alonso, G., Johnston, S.T. and Pastor-Galán, D., 2013. Kinematic constraints on buckling a lithospheric-scale orocline along the northern margin of Gondwana: A geologic synthesis. *Tectonophysics*, **582**, 25-49.

Zhang, Y.G. and Frantz, J.D., 1987. Determination of the homogenization temperatures and densities of supercritical fluids in the system NaCl-KCl-$CaCl_2$-H_2O using synthetic fluid inclusions. *Chemical Geology*, **64**, 335-350.

FIGURE CAPTIONS

Figure 1. Water phase diagram illustrating the principle of geobarometry based on fluid inclusion T_h and clumped isotope $T\Delta_{47}$ measurements. With known fluid composition and with $T\Delta_{47}$ representing the trapping temperature of fluid inclusions (T_t), the pressure of carbonate crystallization can be obtained from ΔT.

Figure 2. Structural sketch map of the Bodón Unit adapted from Alonso *et al.* (2009) and Muñoz Quijano (2015). The map shows the locations of samples analyzed in this study. Inset shows location of the Bodón Unit on a map of the Iberian Peninsula.

Figure 3. (A) Outcrop photograph of zebra textures developed in well-bedded dolomitized mudstones. (B) Zebra texture displayed on polished and stained hand specimen. Calcite is stained in red. (C) Cathodoluminescence image of dolomite crystals making up the zebra texture. Orange calcite cement is visible in the upper part of the image. (D) Outcrop photograph of a breccia pocket in wel-bedded dolomitized mudstones. Bedding surfaces are visible in the upper part of the photograph (indicated with black dashed lines). Hammer for scale (black arrow). (E) Breccia texture displayed on polished and stained hand specimen. Calcite is stained in red. (F) Cathodoluminescence image of dolomite cement in breccia. Note the large crystal size and stepwise crystal terminations (white arrows). (G) Outcrop photograph of bedding surface of coarse crystalline and Fe-rich dolomite. (H) Breccia texture displayed on polished hand specimen. (I) Photomicrograph (crossed polarized light) of saddle dolomite crystals in coarse crystalline and Fe-rich dolomite.

Figure 4. Graph showing relationship between the modes of fluid inclusion homogenization temperatures (T_h) and clumped isotope (Δ_{47}) temperatures. T_h-values range between 95 and 145°C. Error bars correspond to Q1 – Q3 ranges (25^{th} – 75^{th} percentiles; see table 1). Δ_{47} temperatures range between 107 and 168°C. Error bars correspond to ±1SE (see table 1). The black dashed line represents a 1:1 fit between both temperatures, while the blue dashed lines represent offsets in Δ_{47} temperature (A: +10°C; B: +20°C; C: +30°C). 'ReXX' refers to recrystallized dolomite.

Figure 5. Pressure-temperature phase diagram of saline water. T_h modes obtained for each sample are plotted on the liquid-vapor curve (dashed line), and corresponding isochores have been drawn. $T\Delta_{47}$ values are reported along the isochores of the corresponding samples.

FIGURES:

FIGURE 1:

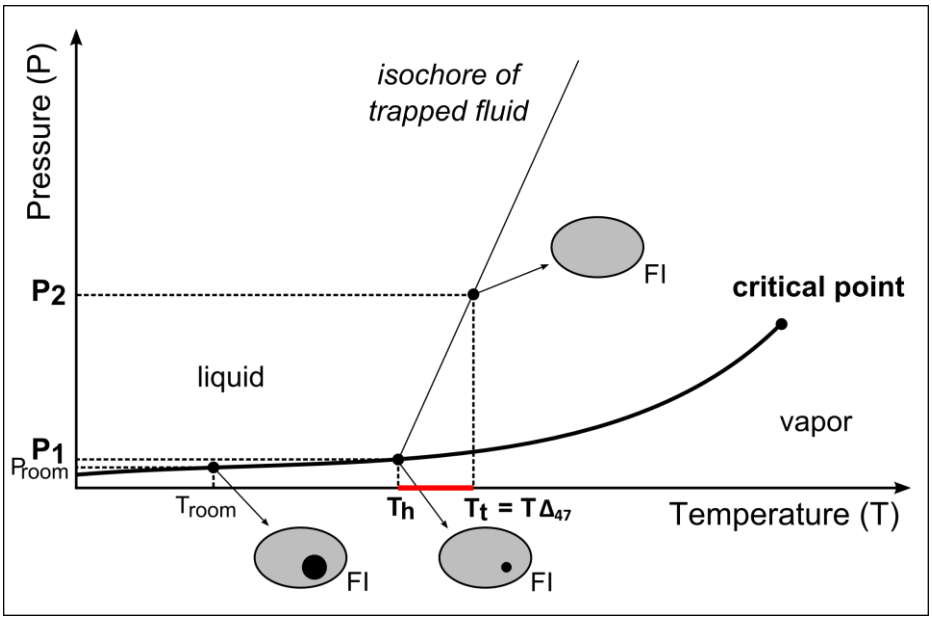

FIGURE 2:

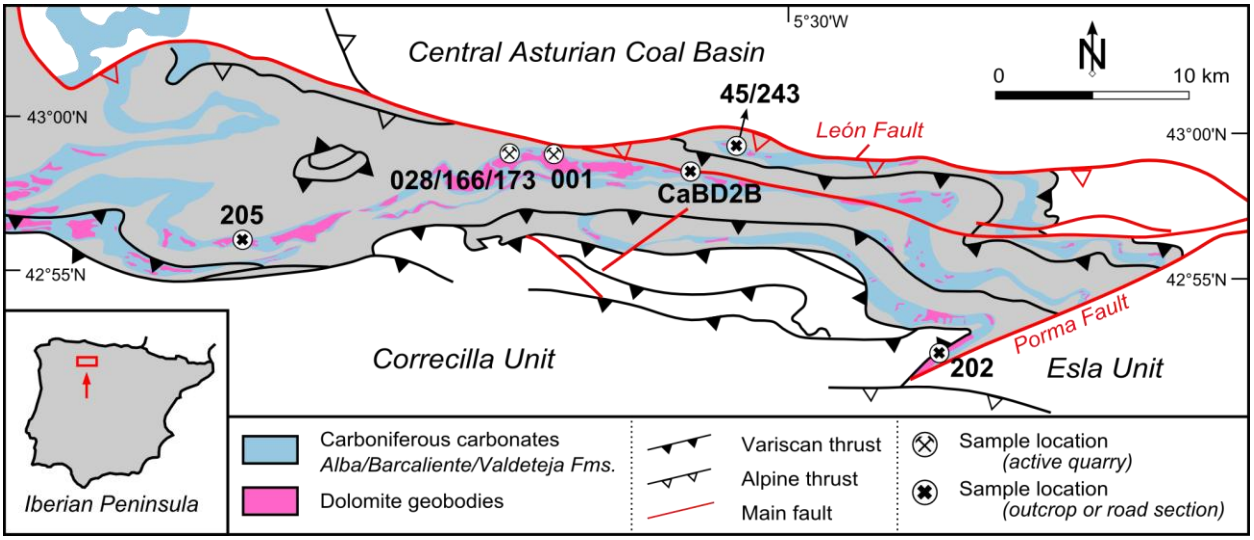

FIGURE 3:

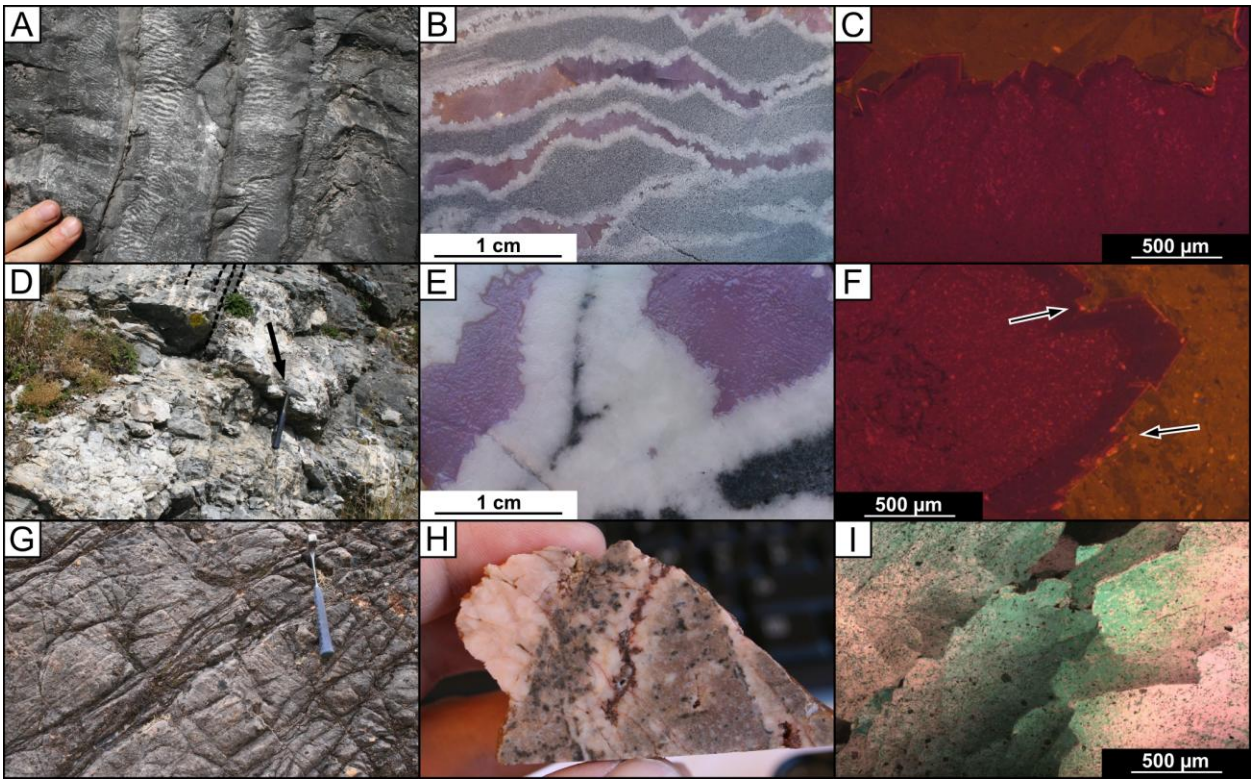

FIGURE 4:

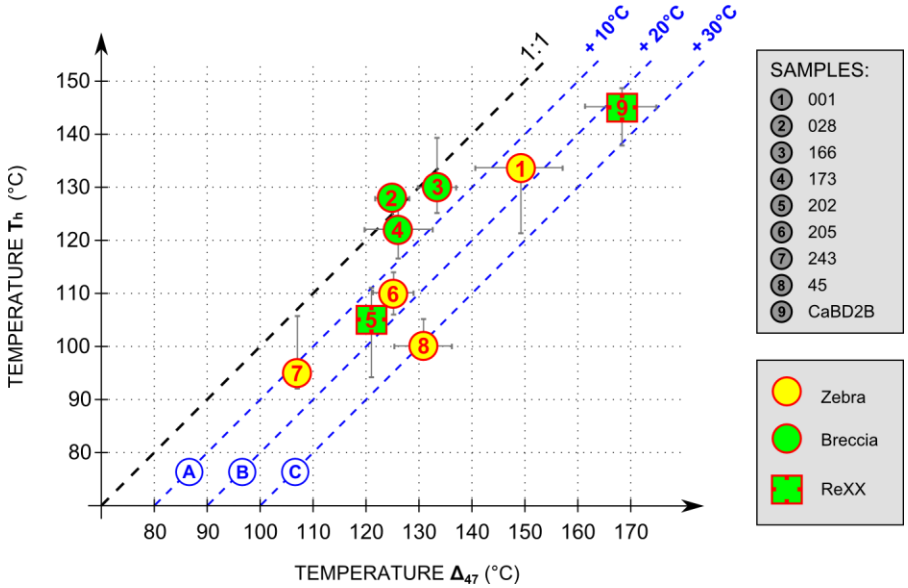

FIGURE 5:

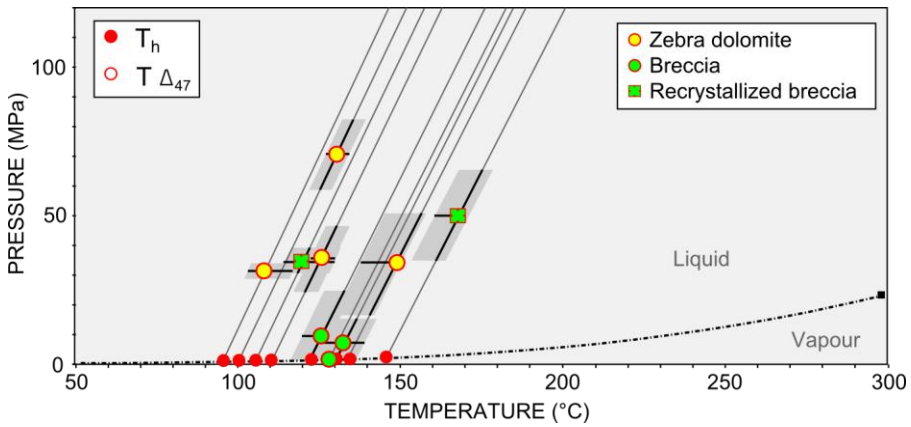

TABLE CAPTION:

Table 1. Results from fluid inclusion microthermometry and clumped isotope paleothermometry. $T\Delta_{47}$ has been calculated using Kluge *et al*. (2015) reprocessed with new parameters for ^{17}O correction (Daëron *et al.*, 2016). Pressure values have been calculated with the equation of state from Zhang and Frantz (1987).

TABLE:

TABLE 1. TEMPERATURE AND CALCULATED PRESSURE VALUES

Sample	Texture	T_h (°C) mode	T_h (°C) range	T_h (°C) Q1 - Q3	# inclusions	$\delta^{13}C$ (‰VPDB)	$\delta^{18}O$ (‰VPDB)	Δ_{47} (‰CDES)	Δ_{47} average	T Δ_{47} (°C)*	±1SE (°C)	±1SD (°C)	±1CL (°C)	P (MPa)
001	Zebra	133	108-151	122-135	56	4.14	-10.17	0.466	0.462	149	8	14	34	31
								0.474						
								0.447						
028	Breccia	128	102-141	124-129	33	4.35	-9.58	0.495	0.489	125	3	6	14	0
								0.491						
								0.481						
166	Breccia	130	102-154	125-139	103	4.53	-8.24	0.482	0.48	133	4	8	14	7
								0.483						
								0.487						
								0.467						
173	Breccia	123	104-138	117-126	45	3.62	-9.52	0.495	0.489	126	7	16	20	9
								0.520						
								0.467						
								0.479						
								0.483						
202	Breccia	105	79-139	95-111	127	3.3	-6.06	0.489	0.494	121	2	3	7	37
								0.495						
								0.497						
205	Zebra	110	99-125	107-115	54	3.52	-11.3	0.494	0.489	125	4	6	54	34
								0.484						
243	Zebra	95	86-128	70-167	50	3.38	-8.34	0.515	0.513	107	1	1	3	29
								0.514						
								0.511						
45[†]	Zebra	100	88-119	98-106	52	3.64	-8.55	0.481	0.482	131	5	9	22	72
								0.471						
								0.493						
CaBD2B[†]	Breccia	145	129-160	138-148	41	4.23	-9.76	0.438	0.444	168	7	9	93	50
								0.450						

*Calculated using Kluge *et al.* (2015), reprocessed with new parameters for ^{17}O correction (Daëron *et al.*, 2016)

[†]Samples from Gasparrini *et al.* (2006a)